Tubulin glycylation controls primary cilia length

Sudarshan Gadadhar,[1,2] Hala Dadi,[3] Satish Bodakuntla,[1,2] Anne Schnitzler,[4] Ivan Bièche,[4,5] Filippo Rusconi,[3] and Carsten Janke[1,2]

[1]Institut Curie, Paris Sciences et Lettres Research University and [2]Université Paris Sud, Université Paris-Saclay, Centre National de la Recherche Scientifique UMR3348, Orsay, France
[3]Université Paris Sud, Université Paris-Saclay, Centre National de la Recherche Scientifique UMR8000, Orsay, France
[4]Department of Genetics, Institut Curie, Paris Sciences et Lettres Research University, Paris, France
[5]Université Paris Descartes, Sorbonne Paris Cité, Paris, France

As essential components of the eukaryotic cytoskeleton, microtubules fulfill a variety of functions that can be temporally and spatially controlled by tubulin posttranslational modifications. Tubulin glycylation has so far been mostly found on motile cilia and flagella, where it is involved in the stabilization of the axoneme. In contrast, barely anything is known about the role of glycylation in primary cilia because of limitations in detecting this modification in these organelles. We thus developed novel glycylation-specific antibodies with which we detected glycylation in many primary cilia. Glycylation accumulates in primary cilia in a length-dependent manner, and depletion or overexpression of glycylating enzymes modulates the length of primary cilia in cultured cells. This strongly suggests that glycylation is essential for the homeostasis of primary cilia, which has important implications for human disorders related to primary cilia dysfunctions, such as ciliopathies and certain types of cancer.

Introduction

Microtubules (MTs) are key cytoskeletal components that play a variety of essential roles in virtually every eukaryotic cell. An emerging mechanism that could control and coordinate different MT functions is the tubulin code, which is generated by differential expression of tubulin genes (isotypes) and by tubulin posttranslational modifications (PTMs; Janke, 2014). A hotspot of tubulin PTMs is the axoneme, the core structure of cilia and flagella (Konno et al., 2012). Out of the many PTMs found on axonemal MTs, glycylation is particular, as it has so far almost exclusively been detected in motile cilia and flagella (Redeker et al., 1994; Rüdiger et al., 1995; Bré et al., 1996; Weber et al., 1996; Xia et al., 2000). Functional studies in different model organisms strongly suggest that glycylation controls the stability of the axoneme in motile cilia (Rogowski et al., 2009; Wloga et al., 2009; Pathak et al., 2011; Bosch Grau et al., 2013).

In mammals, glycylation is catalyzed by the enzymes of the tubulin tyrosine ligase-like (TTLL) family. Two enzymes, TTLL3 and TTLL8, are initiating glycylases that link the first glycine residues to the modification sites on tubulin, whereas TTLL10 is thought to only elongate preformed glycine chains, giving rise to polyglycylation (Rogowski et al., 2009). Glycylation generated by TTLL3 and TTLL8 is essential for axonemal stability, as codepletion of the two enzymes leads to disassembly of motile cilia in ependymal cells (Bosch Grau et al., 2013). In contrast, polyglycylation appears to be nonessential despite its evolutionary conservation (Bré et al., 1996), as in humans, the polyglycylase TTLL10 is inactive (Rogowski et al., 2009). In contrast to motile cilia, where glycylation has been reliably detected with the monoclonal antibody TAP952 (specific to monoglycylation; Bré et al., 1996, 1998), the same antibody failed to detect the modification in most primary cilia. Consequently, glycylation was widely considered a PTM specific to motile cilia; however, the first indications exist that the modification is present at least in some primary cilia (Davenport et al., 2007). We recently demonstrated that depletion of glycylating enzymes TTLL3 and TTLL8 leads to a partial loss of primary cilia in cultured fibroblasts. In the colon, where TTLL3 is the sole glycylase expressed, the absence of this enzyme leads to a decrease in the number of primary cilia. Strikingly, primary cilia in fibroblasts and colon tissues were not labeled with TAP952, leaving open the question of the presence and role of glycylation in primary cilia (Rocha et al., 2014).

Here, we have raised and characterized new antibodies specific to glycylation, which, in contrast to TAP952, label primary cilia. Using these novel antibodies, we demonstrate that the glycylation of primary cilia is generated progressively after cilia assembly and accumulates with increasing ciliary length. It thus appears that glycylation might stabilize primary cilia, similar to its function in motile cilia. To demonstrate this, we depleted glycylating enzymes in cultured cells and showed a significant shortening of primary cilia. In contrast, overexpression of cilia-targeted TTLL3 leads to an increase in cili-

Correspondence to Carsten Janke: Carsten.Janke@curie.fr

Abbreviations used: CLS, ciliary localization signal; MT, microtubule; MTSB, MT stabilizing buffer; PTM, posttranslational modification; qRT-PCR, quantitative RT-PCR; TTLL, tubulin tyrosine ligase-like.

Supplemental material can be found at:
http://doi.org/10.1083/jcb.201612050

The Rockefeller University Press
J. Cell Biol.
https://doi.org/10.1083/jcb.201612050

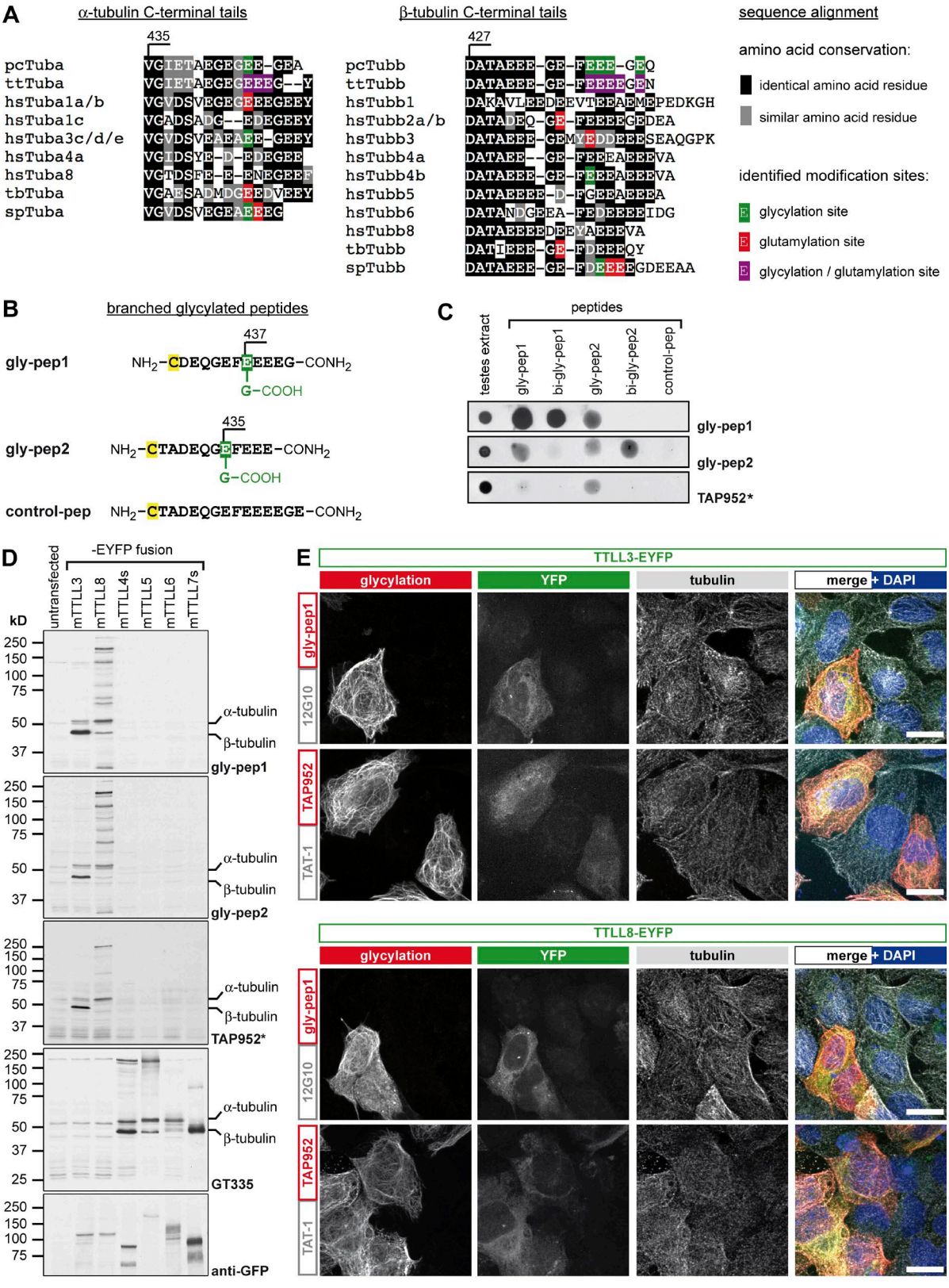

Figure 1. **Generation of a new glycylation-specific antibody.** (A) Multiple sequence alignment of the protein sequences of C-terminal tails of different α- and β-tubulin isotypes from humans compared with different species. Known sites for glycylation (green), glutamylation (red), or both PTMs (purple) are indicated according to the published data: pcTuba, pcTubb (Redeker et al., 1994; Vinh et al., 1997); ttTuba, ttTubb (Redeker et al., 2005); hsTuba1 (Eddé et al., 1990); hsTuba3, hsTubb4b (Plessmann and Weber, 1997); spTuba, spTubb (Mary et al., 1996; Multigner et al., 1996); tbTuba, tbTubb (Schneider et al., 1997); hsTubb2 (Rüdiger et al., 1992); and hsTubb3 (Alexander et al., 1991). pc, *Paramecium cauda*; tt, *Tetrahymena thermophila*; hs, *Homo sapiens;* tb, *Trypanosoma brucei;* sp, *Strongylocentrotus purpuratus*. (B) Glycylated peptides were designed based on human β2-tubulin with glycylation (green) at E437 (gly-pep1) or E435 (gly-pep2) and without glycylation for control (control-pep). The peptides contain a carboxy group at the branched secondary-chain

ary length. Together, our findings demonstrate that glycylation is a tubulin PTM important for the maintenance and length control of primary cilia.

Results and discussion

Generation and validation of novel antibodies to glycylation

So far, cell biology research on tubulin glycylation has relied on two monoclonal antibodies, TAP952 and AXO49, which were both generated using tubulin from the ciliate *Paramecium tetraurelia* as an antigen (Levilliers et al., 1995; Bré et al., 1996). A detailed characterization of the epitopes recognized by these antibodies revealed that TAP952 specifically detects glycylation sites with one single glycine (monoglycylation; Bré et al., 1998), whereas AXO49 detects glycine chains of three or more glycine residues (polyglycylation). A more recently introduced polyclonal antibody, polyG (Xia et al., 2000), detects glycine chains of four or more glycine residues (Tort et al., 2014). All these antibodies reliably stain motile cilia in a wide variety of eukaryotes (Bré et al., 1996; Bosch Grau et al., 2013), demonstrating that they are primarily not species selective and that both mono- and polyglycylation coexist on axonemal MTs, with the exception of humans, in which polyglycylation is absent (Rogowski et al., 2009).

In stark contrast to the reliable detection of monoglycylation in virtually all types of motile cilia, TAP952 does not label primary cilia in most cultured cells. So far, only one study has reported TAP952 staining of cilia in neuronal tissues (Davenport et al., 2007), whereas cilia in other tissues were not stained with this antibody (Rocha et al., 2014). TAP952 was raised against *P. tetraurelia* tubulin (Callen et al., 1994), where it specifically detects glycylated E437, E438, E439, E441, and in particular the combination of all these modification sites on β-tubulin (Bré et al., 1998). We compared these sites with potential modification sites of various tubulin isotypes across species by multiple sequence alignment of α- and β-tubulin tails. As glycylation and glutamylation can occur on similar modification sites, we have labeled all potential sites that have so far been described in the literature (Fig. 1 A). Our alignment shows that there is a range of known modification sites with varying surrounding sequence motives, and not all these potential modification sites align with the previously mapped TAP952 sites (Bré et al., 1998). In particular, β2-Tubulin, one of the major β-tubulin isotypes expressed in mammals, shows a divergent amino acid sequence in the region that is prone to either glycylation or glutamylation (E435 and E437) in different species analyzed so far (Fig. 1 A). It is thus possible that TAP952 does not detect all possible glycylation sites on mammalian tubulin, which is why we decided to raise novel glycylation-specific antibodies.

We synthesized two glycylated peptides that mimic the C-terminal tail of β2-tubulin, gly-pep1 (monoglycylated at E437; Fig. 1 B and Fig. S1 B) and gly-pep2 (monoglycylated at E435; Fig. 1 B and Fig. S1 C). Antibodies raised against these peptides were tested for specificity by spot blot against all glycylated peptides, including biglycylated forms of gly-pep1 and gly-pep2 (Fig. 1 C and Fig. S1, D and E). Both anti–gly-pep1 and anti–gly-pep2 (named gly-pep1 and gly-pep2) were highly specific to their initial, monoglycylated antigens, but also to the respective biglycylated peptides (Fig. S1, D and E). The antibodies also cross-reacted with other monoglycylated peptides, but not with the unmodified peptide (control-pep; Fig. 1 B and Fig. S1 A), underpinning their specificity to glycylation. Strikingly, TAP952 detected both peptides very weakly only after overnight incubation with unusually high antibody concentrations (Fig. 1 C).

To test the specificity of the novel antibodies for glycylation, we analyzed extracts from HEK293 cells expressing YFP-tagged glycylases TTLL3 and TTLL8 (Rogowski et al., 2009) and glutamylases TTLL4, TTLL5, TTLL6, and TTLL7 (van Dijk et al., 2007) by immunoblot. Gly-pep1, gly-pep2, and TAP952 detected specific protein bands in cells overexpressing glycylases, but not glutamylases (Fig. 1 D). Glutamylation was verified with GT335 (purified mouse monoclonal antibody). Strikingly, the principal protein band glycylated by TTLL3 corresponds to β-tubulin, whereas TTLL8 generates many glycylation-specific protein bands including α-tubulin, showing that our novel antibodies detect a range of glycylated proteins. The presence of nontubulin substrates of glycylation has been previously reported (Lalle et al., 2006; Xie et al., 2007; Ikegami et al., 2008; Rogowski et al., 2009), but most of these proteins have so far remained unidentified.

To test our new antibodies in immunofluorescence, we transfected U2OS cells with YFP-tagged TTLL3 and TTLL8 and labeled for glycylated and total tubulin. Similar to TAP952, gly-pep1 selectively stained the MT cytoskeleton in YFP-positive cells, whereas untransfected cells remained completely unlabeled (Fig. 1 E). Gly-pep2, in contrast, generated a diffuse, nonspecific staining in immunofluorescence (not depicted). Thus, we chose to carry on with gly-pep1 antibody, which we purified using a column with immobilized gly-pep1 peptide as the affinity matrix (Fig. S1, F and G).

Glycylation of primary cilia

To determine to what extent the gly-pep1 antibody detects glycylation in primary and motile cilia, we used ependymal cell cultures (Spassky et al., 2005). Strikingly, gly-pep1 labeled both primary and multiple motile cilia at every stage of ependymal development (Fig. 2, A and B). In contrast, TAP952 did not label short primary cilia and weakly labeled long primary cilia or immature multiple cilia, but it strongly stained mature motile cilia (Fig. 2 B) as described previously (Bosch Grau et

glycine, but not at the C-terminal amino acid of the peptides, to focus antigenicity to the glycylation modification. An additional cysteine (C, yellow) was added for peptide coupling. (C) Spot blot analyses of gly-pep antibodies. 300 nmol of control, mono-, or biglycylated β2-tubulin C-terminal–tail peptides were spotted on nitrocellulose membrane and incubated with gly-pep1, gly-pep2, or TAP952. Testes extract from mice were used as a positive control for glycylation. (D) Immunoblot analyses of HEK293 cell lysates expressing YFP-tagged enzymes of the TTLL family (TTLL3, TTLL8: glycylases [Rogowski et al., 2009]; TTLL4, TTLL5, TTLL6, and TTLL7: glutamylases; short versions of TTLL4 and TTLL7 were used; van Dijk et al., 2007). Blots were probed with gly-pep1, gly-pep2, or TAP952 (*, overnight incubation of TAP952) antibodies for glycylation, with GT335 for glutamylation and with anti-GFP antibody to visualize the expression of the YFP-tagged TTLLs. (E) The specific staining of glycylation antibodies to glycylated MTs was tested by immunofluorescence staining of U2OS cells transfected with YFP-tagged TTLL3 or TTLL8 glycylases. Fixed cells were stained with gly-pep1 or TAP952 (red) and for tubulin (12G10 or TAT-1; gray). Bars, 10 µm.

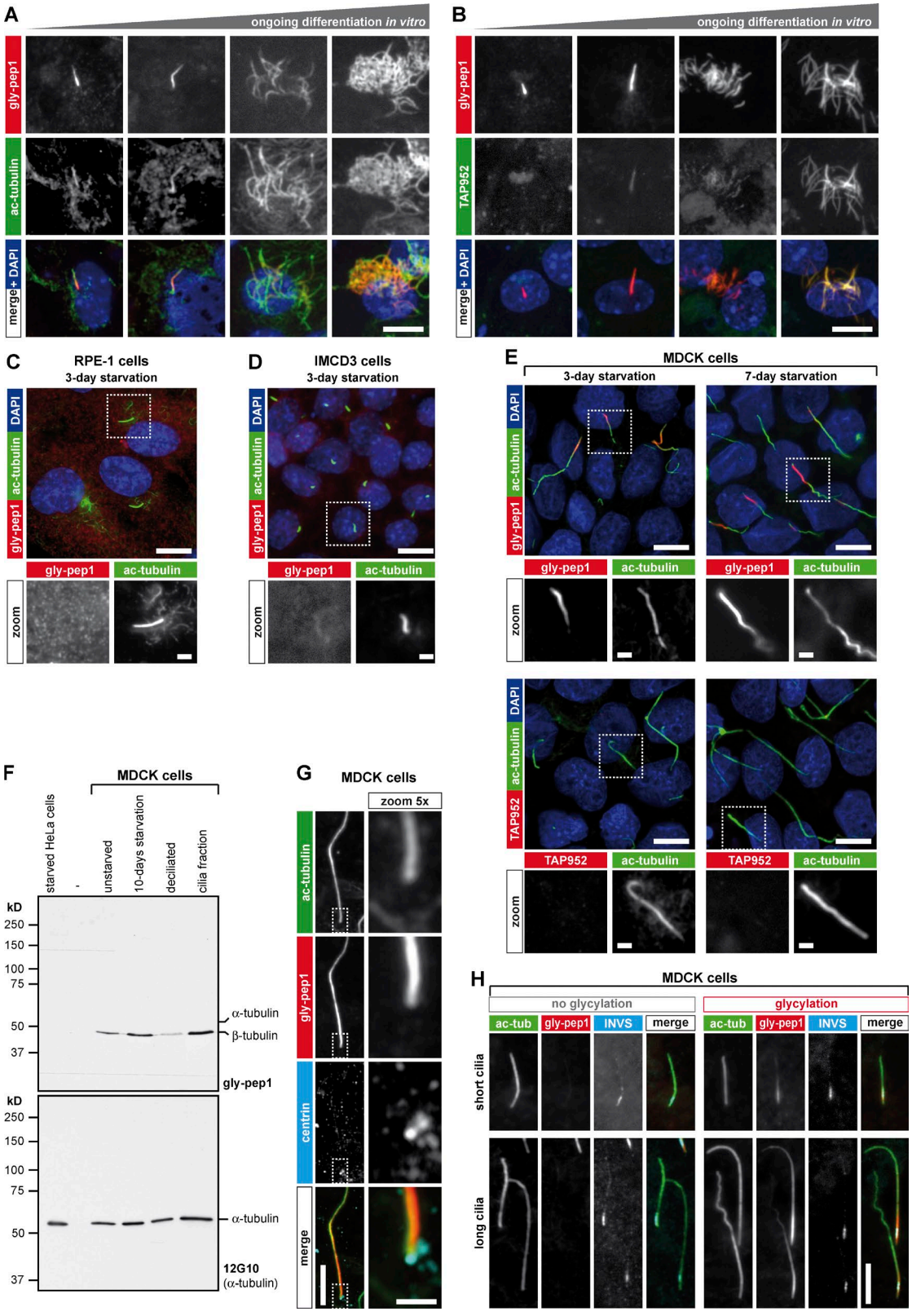

Figure 2. **Gly-pep1 antibody labels motile and primary cilia.** (A and B) Radial glial cells isolated from 1-d-old WT mice were differentiated to ependymal multiciliated cells in vitro for different time periods, and glycylation was monitored with gly-pep1 (red) combined with ac-tubulin (green) to determine ciliary length (A), or with TAP952 (green; B). Whereas gly-pep1 specifically labels primary and motile cilia, TAP952 only labels fully developed multiple motile cilia at a later stage of differentiation. (C and D) RPE-1 cells (C) and IMCD3 cells (D) were serum starved for 3 d and stained with gly-pep1 (red) and ac-tubulin (green). None of the primary cilia in these two cell lines were gly-pep1 positive. (E) MDCK cells were serum starved for 3 or 7 d and stained with either gly-pep1 or TAP952 (red) together with ac-tubulin (green). Note that gly-pep1 but not TAP952 specifically labels primary cilia. (F) Immunoblot analysis of tubulin glycylation in MDCK cells. Extracts of unstarved, 10-d–serum-starved, and starved and deciliated MDCK cells were analyzed together

al., 2013). We next analyzed the cell lines MDCK (dog kidney cells), IMCD3 (mouse kidney cells), and RPE-1 (human retinal epithelial cells), which grow primary cilia after serum starvation (Plotnikova et al., 2009). IMCD3 and RPE-1 cells grew relatively short primary cilia, which were not detected with gly-pep1 (Fig. 2, C and D). In contrast, MDCK cells grew very long primary cilia, which were often stained with gly-pep1, but never with TAP952 (Fig. 2 E). Thus, the novel gly-pep1 antibody revealed the presence of posttranslational glycylation in primary cilia.

To investigate whether the glycylation signal in the primary cilia of MDCK cells originates from glycylated MTs, we deciliated 10-d-starved MDCK cells with $(NH_4)_2SO_4$ for 3 h (Overgaard et al., 2009). We collected the detached cilia (and floating cells) from the cell culture medium by centrifugation and compared this fraction with extracts of unstarved, starved, and deciliated MDCK cells by immunoblot. Starved HeLa cells, which do not grow cilia, were included as a negative control. All fractions were analyzed with gly-pep1 in immunoblots, which detected a specific protein band at ∼50 kD, the size of β-tubulin. Although this band was not detected in HeLa cells, it was already present in the unstarved MDCK cells and increased in intensity upon induction of ciliogenesis. When MDCK cells were deciliated, the signal decreased and was recovered in the ciliary fraction (Fig. 2 F). This indicates that most of the glycylated tubulin is found in the primary cilia of MDCK cells. As no other gly-pep1–positive protein was detected, it is likely that the gly-pep1 labeling of the primary cilia (Fig. 2 E) originated exclusively from the glycylation of axonemal MTs.

The glycylation signal in primary cilia was unevenly distributed: it was most prominent at the proximal part of the cilia, as visualized by costaining of the basal body (centrin; Fig. 2 G). However, it was not confined to the well-defined ciliary transition zone (Czarnecki and Shah, 2012), which we visualized by expressing the transition zone–specific protein inversin (3× FLAG-INVS; Czarnecki et al., 2015) in MDCK cells (Fig. 2 H).

Glycylation of primary cilia accumulates on cilia with increasing length

To determine the kinetics of glycylation in primary cilia, MDCK cells were starved for 1 or 3 d, and their length was determined by measuring the acetylated-tubulin (ac-tubulin) signals (Fig. 3 A). At both time points, a range of different cilia lengths was present, indicating that the ciliation process was asynchronous (Fig. 3 B). However, the percentage of cilia with a clear gly-pep1 signal was consistently low for short cilia and increased with the length of cilia (Fig. 3 C). Although the same trend was found after 1 and 3 d of starvation, slightly higher numbers of cilia were glycylation positive after 3 d. It thus appears that glycylation is mostly length dependent; however, we could not exclude the possibility that shorter cilia are not glycylated because the machinery necessary for glycylation is not fully available at the beginning of ciliation.

To test this possibility, we repeated our analyses with cells that had already been ciliated and in which a second round of ciliogenesis was reinduced after chemical deciliation. MDCK cells were allowed to ciliate for 2 d, treated with 30 mM $(NH_4)_2SO_4$ for 3 h for complete deciliation, and subsequently allowed to reciliate (Fig. 3 D). 1 d after deciliation and restarvation, MDCK cells had grown predominantly short primary cilia, whereas after 3 d, most cilia had grown longer (Fig. 3, D and E). Strikingly, we found a very similar length–glycylation correlation as in the nonsynchronously ciliated cells: shorter cilia were less glycylated than longer cilia, and a slight accumulation of glycylation in shorter cilia was observed after 3 d of starvation (Fig. 3, compare F with C). Together, these results demonstrate that glycylation, as detectable with gly-pep1 antibody, accumulates in primary cilia in a predominantly length-dependent manner and might play a particularly important role for longer cilia.

This also suggests that glycylation was not detected in cilia of IMCD3 or RPE-1 cells (Fig. 2, C and D) because these cells grew only short cilia. To test this hypothesis, we let IMCD3 cells ciliate for 2 d and then treated them with 50 mM LiCl to increase ciliary length (Miyoshi et al., 2009, 2011; Thompson et al., 2016). Ciliary length was determined after 12, 24, and 36 h of LiCl incubation (Fig. 4 A) and compared with untreated controls. Although in controls, most cilia remained shorter than 3 µm, the presence of LiCl led to a progressive elongation of cilia, with some cilia growing even longer than 6 µm (Fig. 4 B). Strikingly, at 36 h after the addition of LiCl, cilia again became shorter, an effect that had previously been reported (Miyoshi et al., 2009).

IMCD3 cilia were overall less strongly labeled with gly-pep1 as compared with MDCK cilia (compare Fig. 3, A and D; and Fig. 4 A, red), but the number of gly-pep1–positive cilia increased with ciliary length in both LiCl-treated and control IMCD3 cells (Fig. 4 C). Strikingly, a much higher percentage of cilia was stained with gly-pep1 in all length categories in cells treated for 36 h with LiCl. It is possible that this reflects an accumulation of glycylation in the LiCl-induced elongated cilia, which reached their maximum length at 24 h and began to shrink at 36 h (Fig. 4 D) without losing their glycylation (Fig. 4 C). Thus, chemically induced elongation of primary cilia can induce glycylation in previously nonglycylated, short cilia.

Glycylation controls the length of primary cilia

The correlation between the length of primary cilia and the presence of glycylation detected with the antibody gly-pep1 suggests that glycylation could be implicated in the control of ciliary length, perhaps by stabilizing the axonemes as previously proposed for motile cilia (Wloga et al., 2009; Bosch Grau et al., 2013), sperm flagella (Rogowski et al., 2009), and connecting cilia of photoreceptors (Bosch Grau et al., 2017). To test this hypothesis, we aimed to deplete glycylation from MDCK cells. MDCK cells express detectable, though low, amounts of *TTLL3* (Fig. S2 A), whereas no expression of *TTLL8* could be detected

with the cilia fraction from the deciliated cells using gly-pep1 antibody and 12G10. Starved HeLa cells were used as a negative control. (G) Serum-starved MDCK cells were stained with gly-pep1 (red), 6–11-B1 (ac-tubulin; green), and 20H5 (pan-centrin; cyan). The gly-pep1 staining was localized in the vicinity of the centrin-stained basal body, indicating that glycylation accumulates at the proximal part of primary cilia. Note that the centrioles are not stained with gly-pep1, indicating that only axonemal MTs undergo glycylation. (H) MDCK cells transduced with 3× FLAG-INVS were colabeled with gly-pep1 (red), 6–11-B1 (ac-tubulin; green), and anti-FLAG antibody (cyan). Note that irrespective of the length of the cilia (ac-tubulin) or of the absence or presence of glycylation (gly-pep1), the size of the inversin segment was identical. Bars, 10 µm; magnified images, 2 µm.

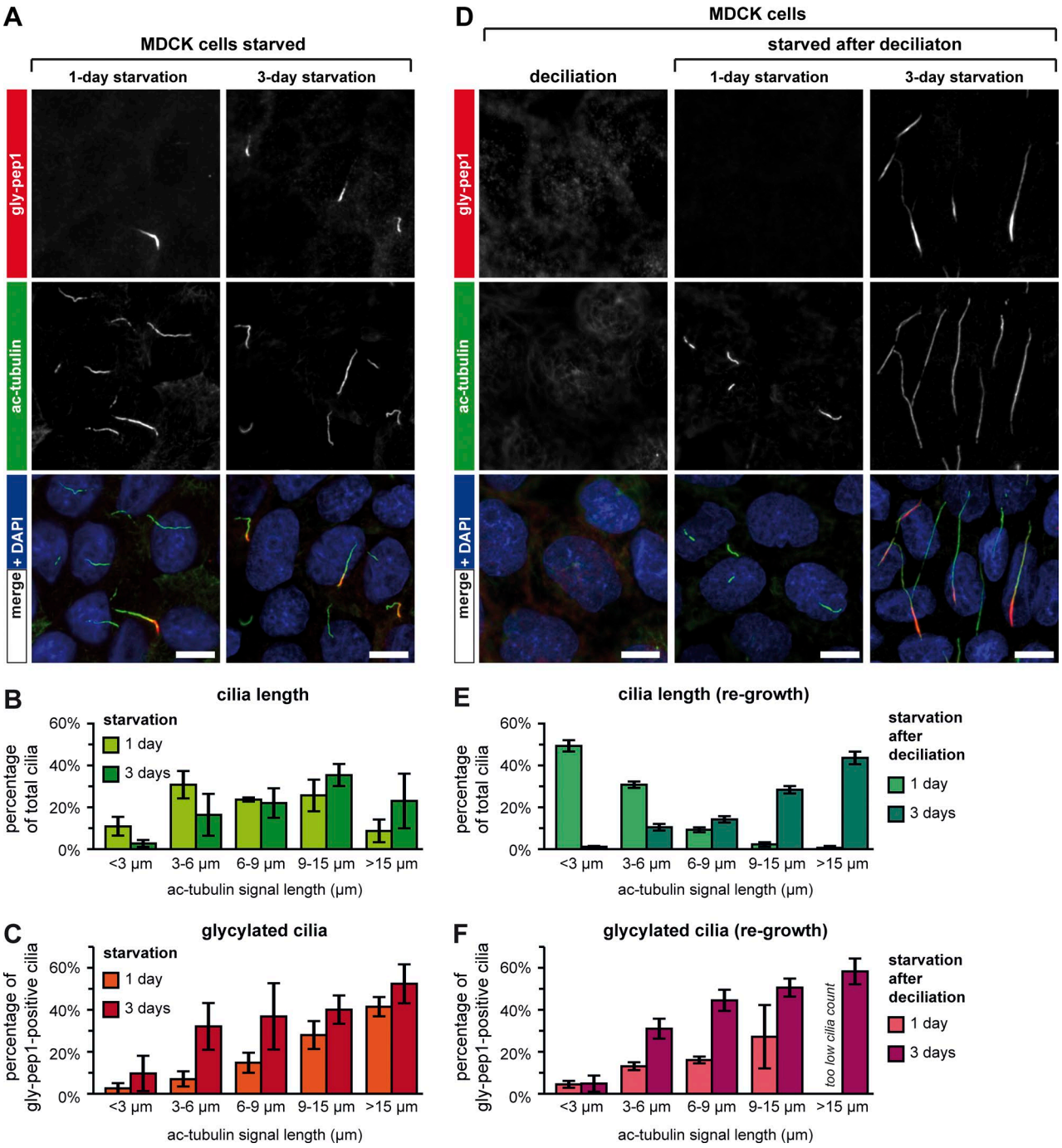

Figure 3. **Glycylation in primary cilia of MDCK cells is length dependent.** (A) MDCK cells were serum starved for 1 or 3 d and analyzed by immunostaining with ac-tubulin (green) and gly-pep1 (red) antibodies. (B) Quantification of ciliary length (length of ac-tubulin signal in A) from MDCK cells starved for 1 or 3 d. The graph represents the percentage of cilia for each length category. Each bar represents the mean of three independent experiments (±SD). (C) Graphic representation of the percentage of gly-pep1–positive cilia for each length category. Each bar represents the mean of three independent experiments (±SD), using the same images that were quantified in B. (D) Immunofluorescence analysis of serum-starved MDCK cells after a cycle of ciliation–deciliation. After deciliation, cells were restarved for 1 or 3 d and stained for ac-tubulin (green) and glycylation (red). Note that upon deciliation, all cells lost their cilia. Bars, 10 µm. (E) Quantification of ciliary length in deciliated and reciliated cells, which were analyzed as described in B. (F) Percentage of glycylated (gly-pep1) cilia in deciliated and reciliated cells analyzed as described in C.

(not depicted). We thus knocked down *TTLL3* expression in MDCK cells using lentiviral shRNA constructs. All three shRNAs led to a reduction of *TTLL3* expression (Fig. S2 A), and cilia were remarkably shorter in *TTLL3*-shRNA–treated cells as compared with the scramble control, with TTLL3_994 having the strongest impact on ciliary length (Fig. 5, A and B; and Fig. S2, B, C, and E). In both *TTLL3*-shRNA– and scramble-shRNA–treated cells, the percentage of glycylated cilia was consistently higher when cilia were longer (Fig. 5 C and Fig. S2 D). However, for each length category, the percentage of glycylated cilia was lower in *TTLL3*-shRNA–treated cells as compared with scramble-shRNA (Fig. 5 C and Fig. S2 D), con-

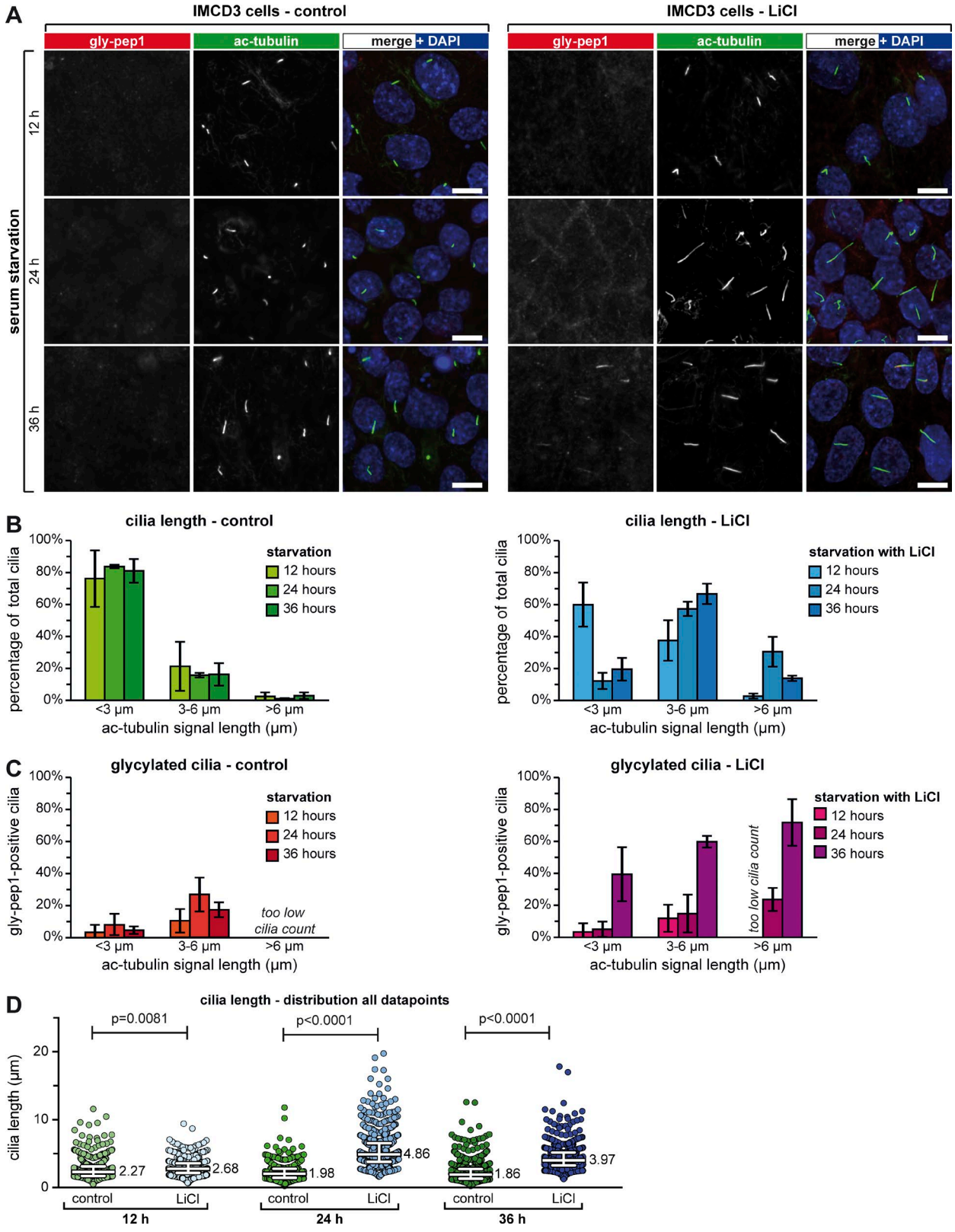

Figure 4. **Elongation of short primary cilia induces their glycylation.** (A) Confluent IMCD3 cells were serum starved in the absence (control) and presence of 50 mM LiCl for 12, 24, and 36 h and stained for ac-tubulin (green) and glycylation (gly-pep1; red). Bars, 10 µm. (B) Quantification of ciliary length for A. The graphs represent the percentage of cilia for each length category. Each bar represents the mean of three independent experiments (±SD). (C) Percentage of gly-pep1–positive cilia in the different length categories, represented as in B. (D) Ciliary length measurements from three independent experiments for each experimental condition shown in A are represented as a scatter plot with a line indicating the median (value indicated) and whiskers at interquartile ranges (25th and 75th percentiles). P-values were calculated by one-way ANOVA. Individual experiments are shown in Fig. S3 A. For the number of individual measurements per data point, see Table S1 ($n > 450$).

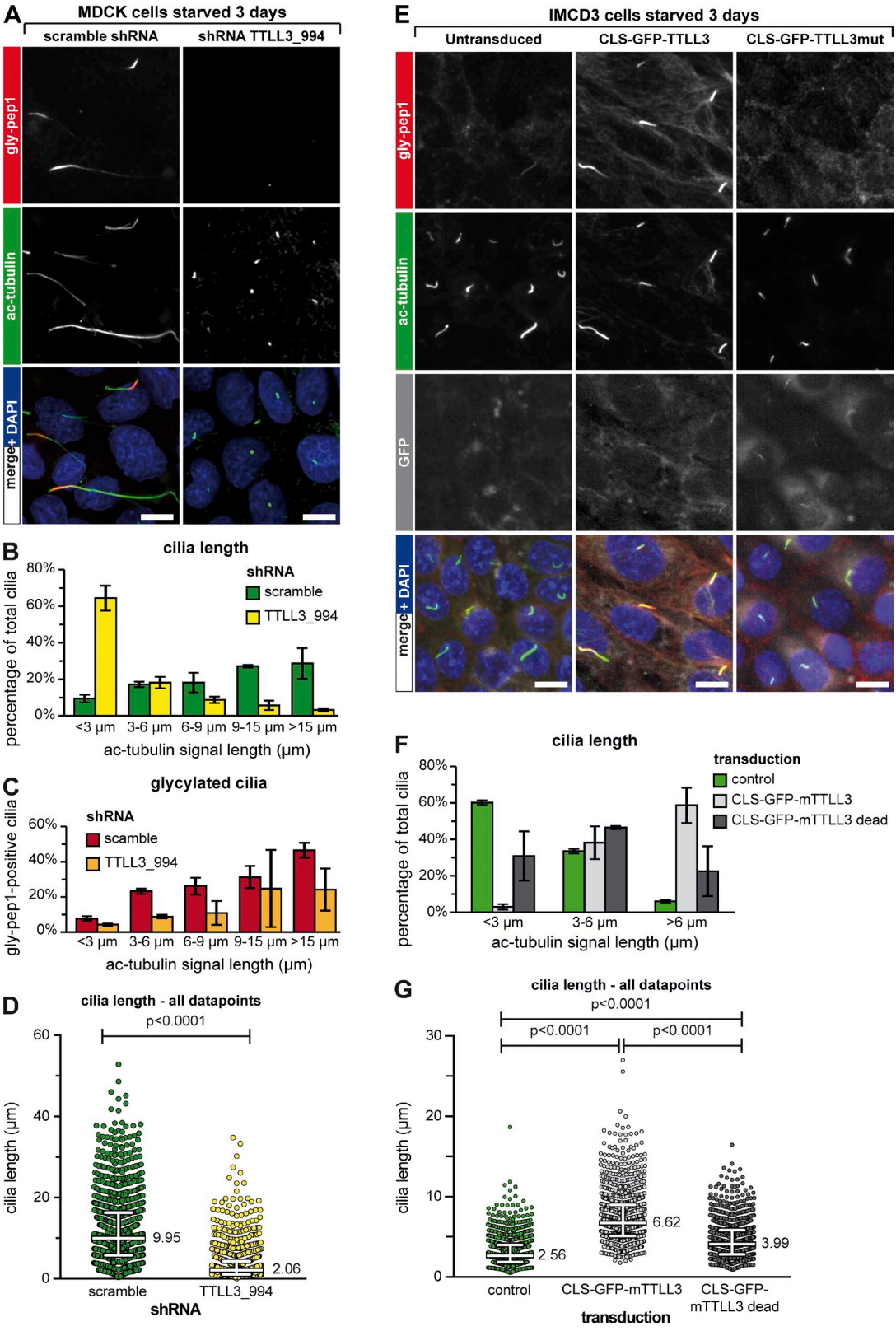

Figure 5. **Glycylation regulates ciliary length.** (A) MDCK cells were transduced with scrambled or TTLL3-specific shRNA constructs (Fig. S2 A) and serum starved for 3 d. Cilia were stained with ac-tubulin (green) and glycylation with gly-pep1 (red). Note the strong decrease of ciliary length in cells treated with shRNA TTLL3_994. Bars, 10 µm. (B) Quantification of the ciliary length for A. The graphs represent the percentage of cilia for each length category. Each bar represents the mean of three independent experiments (±SD). (C) Percentage of gly-pep1–positive cilia was determined for each of the different length groups and plotted as the mean value of three independent experiments (±SD). (D) Ciliary length measurements from three independent experiments for each experimental condition shown in A are represented as a scatter plot with a line indicating the median (value indicated) and whiskers at interquartile ranges (25th and 75th percentiles). P-values were calculated by one-way ANOVA. Individual experiments are shown in Fig. S3 B. For the number of indi-

firming that depletion of *TTLL3* leads to a decrease of glycylation in cilia. This also suggests that the cells that still have longer cilia in *TTLL3*-shRNA–treated samples might have been less efficiently depleted of *TTLL3* than the majority of the cells. Together, these experiments demonstrate that the depletion of glycylation in MDCK cells leads to a significant decrease of ciliary length (Fig. 5 D and Fig. S2 E). In contrast to our previous observations in connecting cilia of photoreceptors, in which the absence of *TTLL3* led to a gradual increase in glutamylation and photoreceptor degeneration (Bosch Grau et al., 2017), the shortening of primary cilia after depletion of glycylation was not accompanied by a detectable up-regulation of glutamylation (GT335; Fig. S2 F). This indicates that the reduction in ciliary length is most likely induced by a mechanism that is directly controlled by glycylation levels of the axonemal MTs.

Finally, we asked whether a forced increase of glycylation in the primary cilia could induce ciliary elongation. Overexpression of glycylation in cultured cells leads to a massive glycylation of the entire MT cytoskeleton and was therefore not appropriate to test the role of glycylation specifically in cilia. We thus generated a lentiviral vector in which we combined a promoter with very low activity (Nager et al., 2017), a ciliary localization signal (CLS) derived from Nephrocystin-3 (Mick et al., 2015), and the GFP-tagged TTLL3 protein or its ATPase-dead mutant. Cells transduced with these constructs and serum starved for 3 d showed a very weak but specific GFP signal in the primary cilia. In the case of TTLL3, this lead to a massive accumulation of glycylation (gly-pep1 signal) in the primary cilia, whereas cytosolic MTs were only faintly glycylated, indicating that our approach of targeting glycylation into cilia had been successful (Fig. 5 E). Expression of CLS-GFP-TTLL3 led to an ∼2.5-fold increase of ciliary length as compared with control (Fig. 5, F and G). However, expression of the CLS-GFP-TTLL3–dead constructs also increased ciliary length, but to a lesser extent (∼1.5-fold over control; Fig. 5, F and G), which is most likely related to the cilia-stabilizing effect of the CLS. The glycylation-related increase of ciliary length (Fig. 5, F and G) demonstrates that this tubulin modification is involved in the control of ciliary length, but it is not sufficient to increase the ciliary length in IMCD3 cells at a scale seen in MDCK cells. Thus, additional mechanisms, which could be directly regulated by the glycylation status of the ciliary axonemes but are absent in IMCD3 cells, might be involved in length scaling of primary cilia.

Conclusions

Primary cilia are key organelles with crucial roles in signaling pathways (Lancaster et al., 2011; Basten and Giles, 2013; Delling et al., 2013; Fry et al., 2014; Malicki and Johnson, 2017), and their dysfunction can lead to ciliopathies (Tobin and Beales, 2009; Hildebrandt et al., 2011; Waters and Beales, 2011; Huber and Cormier-Daire, 2012) or cancer (Michaud and Yoder, 2006; Wong et al., 2009; Han and Alvarez-Buylla, 2010; Basten and Giles, 2013). Despite our initial observations that posttranslational glycylation is important for primary cilia and tissue proliferation (Rocha et al., 2014), this modification was so far almost exclusively detected in motile cilia (Rogowski et al., 2009; Wloga et al., 2009; Pathak et al., 2011; Bosch Grau et al., 2013). Here, we developed a novel antibody, which allowed us to demonstrate the presence of glycylation in primary cilia and also to determine its role in controlling the length of these organelles. Our findings are of key importance for virtually all functions related to cilia and have repercussions for the understanding of the molecular mechanisms of primary cilia functions and their role in a wide range of cilia-related disorders.

Materials and methods

Peptide synthesis and antibody production

The sequences for the C-terminal tail peptides of β2-tubulin were designed with glycylation on the most frequently modified amino acid residues on β-tubulins of different species (Fig. 1 A). Peptides were synthesized using a standard peptide synthesis protocol with a mono- or biglycylated glutamate building block for the modified sites (Fig. 1 B) and were purified by HPLC (Peptide Specialty Laboratory). Peptides were then coupled to keyhole limpet hemocyanin. Antibodies were raised in rabbits (Pettingill Technology). The TAP952 antibody was produced from hybridoma cell lines and purified on a protein G affinity column (17-0405-01; GE Healthcare) with the help of A. Aubusson-Fleury (Institut de Biologie Intégrative de la Cellule, Gif-sur-Yvette, France).

Cell culture and transfection

HEK293(CRL-1573;ATCC),HeLa(CCL-2;ATCC),andU2OS(HTB-96; ATCC) cells were cultured under standard conditions in DMEM/F12 culture media (Thermo Fisher Scientific) containing 10% FBS (Sigma Aldrich). Transfection of expression plasmids was performed using jetPEI (PolyPlus) transfection reagent according to the manufacturer's instructions. Cells were analyzed 20 h after transfection.

For primary ependymal cell culture, we used the published protocol for isolation, culturing, and differentiation (Delgehyr et al., 2015). In brief, cells from the subventricular zone of the brains of newborn pups of WT C57B6/J mice were isolated, dissociated, washed, and plated at high density in DMEM/F12 containing 10% FBS in a 25-cm^2 flask precoated with poly-L-lysine (P4832; Sigma Aldrich). When cells reached confluency, the astroglial monolayer was replated onto precoated 12-mm glass coverslips in 24-well plates at a density of 10^4 cells/µl and maintained in serum-free medium to enable differentiation. Cells were fixed at the different time points, and cells representative of different developmental stages were imaged.

Spot blot and immunoblot analyses

To test the specificity of gly-pep1 and gly-pep2 antibodies, a spot blot analysis modified from Bré et al. (1996) was used. 300 nmol of each synthetic β-tubulin peptide (control, gly-pep1, bi–gly-pep1, gly-pep2, and bi–gly-pep2) was spotted on preactivated nitrocellulose membrane strips and dried for 5 min at 50°C.

vidual measurements per data point, see Table S1 (n > 1,000). (E) IMCD3 cells were transduced with active or mutant TTLL3 fused to GFP and a CLS and serum starved for 3 d. Cilia were stained with ac-tubulin (green) and glycylation with gly-pep1 (red). GFP is depicted in gray. Note the increase in length of cilia positive for gly-pep1 in cells transduced with active TTLL3. (F) Quantification of the ciliary length in control cells and cells transduced with active or mutant TTLL3 as described in D. In transduced cells, only GFP-positive cilia were considered for analyses. (G) Ciliary length measurements from three independent experiments for each experimental condition shown in E are represented as a scatter plot with a line indicating the median (value indicated) and whiskers at interquartile ranges (25th and 75th percentiles). P-values were calculated by one-way ANOVA. Individual experiments are shown in Fig. S3 C. For the number of individual measurements per data point, see Table S1 (n > 1,100).

For immunoblot analyses of cell extracts, HEK293 cells were plated in 6-well plates (7×10^5 cells/well) and transfected with expression plasmids for YFP-fusion proteins of different TTLL proteins (van Dijk et al., 2007; Rogowski et al., 2009) using jetPEI. Cells were harvested 20 h after transfection, directly lysed in SDS sample buffer, and run on 10% SDS-PAGE gels. A specific protocol was used to separate α- and β-tubulin (Magiera and Janke, 2013). In brief, specific SDS-PAGE gels were prepared at 375 mM Tris-HCl, pH 9.0, 0.1% SDS (L5750; Sigma Aldrich), and 10% acrylamide (40% acrylamide solution; 161-0140; Bio-Rad) supplemented with 0.54% bis-acrylamide (wt/vol) powder (161-0210; Bio-Rad). Proteins were transferred to nitrocellulose membranes with Trans-Blot Turbo using transfer packs (1704159; Bio-Rad) and subjected to immunoblot analysis.

Membranes from spot blots and immunoblots were blocked for 1 h with 50 mM TBS with 0.1% Tween 20 (TBS-T) containing 5% nonfat milk and then incubated for 2 h at room temperature (spot blot/immunoblot) with anti–gly-pep1 (purified, 1 mg/ml: 1:2,500/1:5,000; AG-25B-0034; Adipogen Life Sciences), anti–gly-pep2 (rabbit serum, 1:500/1:1,500), and 12G10 (immunoblot, 1:500; antibody developed by J. Frankel and M. Nelson and obtained from the Developmental Studies Hybridoma Bank developed under the auspices of the National Institute of Child Health and Human Development and maintained by the University of Iowa). TAP952 (purified mouse monoclonal antibody, 1 mg/ml: 1:100/1:400) was incubated overnight at 4°C. For glutamylation, immunoblots were incubated with GT335 (purified mouse monoclonal antibody, 1:5,000; AG-20B-0020-C100; Adipogen Life Sciences), and for detecting the expression of YFP-tagged proteins, with polyclonal rabbit anti-GFP antibody (1:5,000; TP401; Torrey Pines Biolabs). Antibodies were diluted in TBS-T containing 2.5% nonfat milk. Membranes were washed four times with TBS-T and then incubated for 1.5 h with goat anti–rabbit (31460; Thermo Fisher Scientific) or anti–mouse (31430; Thermo Fisher Scientific) secondary antibodies conjugated to HRP diluted to 1:10,000 in TBS-T. After washing five times in TBS-T, antibody labeling was revealed using ECL Western blotting detection reagent (GE Healthcare).

Ciliogenesis

RPE-1 (CRL-4000; ATCC), MDCK (CCL-34; ATCC), and IMCD3 (CRL-2123; ATCC) cells were plated on 12-mm glass coverslips in a 24-well plate and cultured to confluency in DMEM/F12 (1:1; Thermo Fisher Scientific) containing 10% FBS. The cells were then washed twice with PBS and cultured in serum-free DMEM/F12 for different time intervals to induce ciliogenesis.

IMCD3 cells for LiCl treatment (Fig. 4) were plated on 12-mm glass coverslips, grown to confluence, and serum starved for 2 d. The cells were then cultured in starvation medium containing 50 mM LiCl (Thompson et al., 2016) for different time intervals (12, 24, and 36 h). A series of control experiments was performed by omitting LiCl.

Deciliation and rescue of ciliogenesis

Deciliation and reciliation experiments were performed as described previously (Overgaard et al., 2009). For Fig. 3 (D and F), MDCK cells were plated on 12-mm glass coverslips and grown to confluence and then cultured in serum-free medium for 2 d to enable ciliogenesis. After ciliation, the cells were washed and incubated in complete medium with 30 mM $(NH_4)_2SO_4$ for 3 h for deciliation. To rescue the cells and enable reciliation, the cells were washed twice with PBS and cultured in serum-free medium for 1 or 3 d.

For the immunoblot analysis of ciliary versus cellular fractions (Fig. 2 F), MDCK cells were starved for 10 d and then deciliated for 3 h. The cell culture medium was harvested and subjected to repeated cycles of centrifugation at 2,000 *g* for 30 min at room temperature. The pellets were resuspended in lysis buffer (20 mM sodium phosphate, pH 7.2, containing 150 mM NaCl, 1 mM EDTA, 10% [vol/vol] glycerol, 1% Triton X-100, and protease inhibitor cocktail). 40 µg of total protein was analyzed by SDS-PAGE and immunoblot with purified gly-pep1 (1:5,000) and 12G10 (1:1,000).

Cell fixation and immunofluorescence

Cells plated on 12-mm glass coverslips in 24-well plates were fixed with a protocol to preserve the cytoskeleton (Bell and Safiejko-Mroczka, 1995). In brief, the cellular proteins were cross-linked using the homobifunctional cross-linker dithiobis(succinimidyl propionate) (22585; Thermo Fisher Scientific) in MT-stabilizing buffer (MTSB) after permeabilization with 0.5% Triton X-100 in MTSB. The cells were then fixed with 4% paraformaldehyde in MTSB and transferred to PBS. For the experiments shown in Fig. 1 E, cells were first fixed and then permeabilized.

Primary ependymal cells and starved MDCK cells used for staining with anti-centrin antibody were permeabilized with 0.1% Triton X-100 in BRB80 (80 mM Pipes/KOH, pH 6.8, 5 mM EGTA, and 5 mM $MgCl_2$) for 90 s and then fixed in ice-cold methanol for 10 min at −20°C and transferred to PBS. Cells were blocked with PBS containing 10% FBS for 1 h at room temperature (Delgehyr et al., 2015).

Primary antibodies were diluted in PBS containing 3% BSA and 0.1% Triton X-100 for 2 h at room temperature. We used purified gly-pep1 (1:5,000), TAP952 (1:1,000), mouse anti-acetylated α-tubulin (1:5,000; TEU318; AG-20B-0068-C100; Adipogen Life Sciences), mouse anti-Arl13b (1:750; N295B/66; NeuroMab), mouse anti–α-tubulin 12G10 (1:1,000) or TAT-1 (1:1,000; 00020911; Public Health England), mouse anti-centrin (1:800; 04-1624, Sigma Aldrich), mouse anti-FLAG (1:1,000; F1804; Sigma Aldrich), and GT335 (1:5,000). For acetylated α-tubulin staining in the ependymal cells, 6–11-B1 (1:1,000; mouse monoclonal; MABT868; Sigma Aldrich) was used. Secondary antibodies were diluted in the same buffer as the primary antibody and incubated for 1 h at room temperature. We used goat anti–rabbit Alexa Fluor 568 (1:1,000; A11036), goat anti–mouse IgG1 Alexa Fluor 488 (1:1,000; A21121), goat anti–mouse IgG2a (1:1,000; A21235), or IgG2b Alexa Fluor 647 (1:1,000; A21242; Thermo Fisher Scientific). Nuclei were visualized by staining for 5 min with DAPI (0.02 µg/ml; D3571; Thermo Fisher Scientific). Coverslips were mounted using ProLong gold antifade medium (P36930; Thermo Fisher Scientific).

TTLL3 knockdown

Lentiviral particles of vectors encoding GFP or RFP together with shRNA under the control of the H1 promoter (shRNA scramble, TTLL3_478, TTLL3_556, or TTLL3_994) were generated by transfecting them into X-Lenti 293T (632180; Clontech) cells together with viral packaging plasmids (psPAX2 and VSV-G) using Trans-IT-293 transfection reagent (MIR 2705; Mirus Bio LLC). 16 h after transfection, the culture medium was replaced by Opti-MEM medium (Thermo Fisher Scientific) for a period of 30 h, allowing virus production. The virus-containing medium was collected, filtered, and stored at −80°C (Lahaye et al., 2013). Virus-containing cell culture media were calibrated for 90–100% transduction efficiency by directly adding different volumes of the media to MDCK cell cultures. The optimal volume for each virus was then used for further experiments.

MDCK cells grown to 50% confluence in complete DMEM/F12 medium were cultured with lentivirus-containing medium for 2 d. Cells were washed extensively with PBS and cultured for an additional 3 d in serum-free medium to enable ciliogenesis. Cells were either harvested for RNA isolation or fixed as described earlier for immunofluorescence.

Target sequences of shRNA were scramble, 5′-TGCGCTACG ATCGACGATG-3′; TTLL3_478, 5′-GAGAGAGCTGTCAAGCAG AAG-3′; TTLL3_556, 5′-GGCTGGGTGGAGAAGAAGATG-3′; or TTLL3_994, 5′-GCCTTCATAGAGGACTTCTGG-3′.

Ciliary targeting with lentivirus expression vectors

Lentiviral constructs of codon-optimized full-length TTLL3 and the ATPase-dead version of TTLL3 were cloned into a lentiviral vector backbone, preceded by a low-activity EF1-α promoter with a mutated TATA box (Nager et al., 2017), the N-terminal region of Nephrocystin-3, which acts as the CLS (Mick et al., 2015), and GFP. Plasmids used for subcloning were provided by D. Mick and M. Nachury (Stanford University, Stanford, CA) and N. Manel (Institut Curie, Paris, France). The lentiviral construct for the expression of flag-tagged inversin (pCDH-EF1-3× FLAG-INVS; Czarnecki et al., 2015) was a gift from J. Shah and P. Czarnecki (Harvard Medical School, Boston, MA). Lentiviral particles were produced as described above, and IMCD3 or MDCK cells were transduced with viruses containing the herein described constructs, grown for 48 h in complete medium, washed, and serum starved for 3 d. Cells were then fixed as described for immunofluorescence analyses.

Microscopy

All microscopy images apart from Fig. 1 E were acquired using a Structured Illumination microscope (Optigrid; Leica Systems) with a 63× (NA 1.40) oil immersion objective at room temperature. Images were acquired using the ORCA-Flash4.0 camera (Hamamatsu) and MM AF imaging software (Leica Systems). For image analysis, the images were processed using ImageJ (National Institutes of Health). Images in Fig. 1 E were acquired with a spinning-disk inverted confocal laser microscope (Ti-E; Nikon) using a 60× oil immersion objective (NA 1.40) at room temperature. Images were acquired using the ORCA-Flash4.0 camera and MM AF imaging software. Multiple Z stacks were acquired, and a maximum intensity projection was prepared using ImageJ v1.51a to generate the final image.

Quantification of cilia and statistics

Images with glycylation and cilia staining were processed in ImageJ v1.51a. Only the intensity of single-color channels was adjusted in a linear manner for better representation in the figures using ImageJ and Photoshop (Adobe), and no additional image treatments were performed. The length of the cilia was determined by measuring the acetylated α-tubulin signals using ImageJ. The percentage of gly-pep1–positive cilia was determined relative to the number of all (ac-tubulin positive) cilia.

For each experimental condition, experiments were performed in triplicates. For ciliation experiments with MDCK cells (Fig. 3), ∼500–1,000 cilia were counted per experiment. For LiCl treatment of IMCD3 cells (Fig. 4), ∼250 cilia were counted per experiment (Fig. S3 A). For ciliary length after *TTLL3* knockdown in MDCK cells (Fig. 5, A–D; and Fig. S2), as well as *TTLL3* overexpression in IMCD3 cells (Fig. 5, E–G), ∼350–450 cilia were counted per condition (Fig. S3, B and C). For IMCD3 cells overexpressing *TTLL3*, only GFP-positive cilia were counted. For each condition, ∼350–400 cilia were counted.

Mean values of individual experiments were plotted in bar graphs with ±SD between the individual sets. Numerical values for each of the quantifications are reported in Table S1.

For statistical analyses of ciliary length, we combined the three experimental replicates and represented all data as scatter plots with a line indicating the median and whiskers at interquartile ranges (25th and 75th percentiles; Fig. 4 D and Fig 5, D and G). P-values were calculated by one-way ANOVA corrected for multiple comparisons using the Tukey statistical hypothesis test using Prism version 7 (GraphPad). Scatter plots for each of the individual experiments are represented in Fig. S3 to demonstrate the reproducibility of the experiments.

Online supplemental material

Fig. S1 describes the validation of the newly synthesized glycylated peptides and the purity of the gly-pep1 antibody. Fig. S2 shows complementary results for the *TTLL3* knockdown analyses described in Fig. 5. Fig. S3 represents the graphs of individual quantification experiments, of which the collective graphs are shown in Fig. 4 D and Fig. 5 (D and G). Table S1 provides the source data for all quantification experiments shown in the manuscript.

Acknowledgments

We thank C. Alberti, E. Belloir, F. Bertrand, T. Giordano, I. Grandjean, H. Hermange, M.M. Magiera, C. Serieyssol, A. Thadal (Institut Curie, Orsay, France), and A. Aubusson-Fleury for technical assistance. We are grateful to A. Aubusson-Fleury for generously providing us essential reagents. We are grateful to J. Shah and P.G. Czarnecki for the lentiviral inversin construct and to M.V. Nachury and D. Mick for the EF1-α-NPHP3 vector, as well as for insightful discussions. We are grateful to M.-N. Soler and C. Lovo from the imaging platform PICT-IBiSA@Orsay (Institut Curie, Orsay, France) for technical assistance in the use of the Leica Structured Illumination Microscope (Optigrid) and the Nikon Eclipse Ti-E inverted microscope systems, and to N. Manel for material and advice for the lentivirus production. We are grateful to M. Bettencourt Dias (Instituto Gulbenkian de Ciência, Oeiras, Portugal), E. Feraille (University of Geneva, Geneva, Switzerland), M. Singh (Indian Institute of Science, Bangalore, India), and M.M. Magiera and P. Singh (Institut Curie, Orsay, France) for instructive discussions and advice.

This work has received support under the program Investissements d'Avenir launched by the French government and implemented by the French National Research Agency (ANR) with the references ANR-10-LBX-0038 and ANR-10-IDEX-0001-02 PSL. The work of C. Janke was supported by the Institut Curie, ANR award ANR-12-BSV2-0007, and the Institut National du Cancer grants 2013-1-PL BIO-02-ICR-1 and 2014-PL BIO-11-ICR-1. H. Dadi received a PhD fellowship from Université Paris Sud/Paris-Saclay, and S. Bodakuntla received a PhD fellowship from the Institut Curie.

The authors declare no competing financial interests.

Author contributions: conceptualization: S. Gadadhar and C. Janke; methodology: S. Gadadhar, F. Rusconi, and C. Janke; software: F. Rusconi; validation: S. Gadadhar, H. Dadi, F. Rusconi, I. Bièche, A. Schnitzler, and C. Janke; formal analysis: S. Gadadhar, S. Bodakuntla, F. Rusconi, A. Schnitzler, and C. Janke; investigation: S. Gadadhar, S. Bodakuntla, and C. Janke; writing, original draft: S. Gadadhar and C. Janke; writing, review and editing: S. Gadadhar, S. Bodakuntla, and C. Janke; visualization: S. Gadadhar and C. Janke; supervision: C. Janke; project administration: C. Janke; funding acquisition: C. Janke.

Submitted: 9 December 2016
Revised: 28 April 2017
Accepted: 24 May 2017

References

Alexander, J.E., D.F. Hunt, M.K. Lee, J. Shabanowitz, H. Michel, S.C. Berlin, T.L. MacDonald, R.J. Sundberg, L.I. Rebhun, and A. Frankfurter. 1991. Characterization of posttranslational modifications in neuron-specific

class III beta-tubulin by mass spectrometry. *Proc. Natl. Acad. Sci. USA.* 88:4685–4689. http://dx.doi.org/10.1073/pnas.88.11.4685

Basten, S.G., and R.H. Giles. 2013. Functional aspects of primary cilia in signaling, cell cycle and tumorigenesis. *Cilia.* 2:6. http://dx.doi.org/10.1186/2046-2530-2-6

Bell, P.B. Jr., and B. Safiejko-Mroczka. 1995. Improved methods for preserving macromolecular structures and visualizing them by fluorescence and scanning electron microscopy. *Scanning Microsc.* 9:843–857.

Bosch Grau, M., G. Gonzalez Curto, C. Rocha, M.M. Magiera, P. Marques Sousa, T. Giordano, N. Spassky, and C. Janke. 2013. Tubulin glycylases and glutamylases have distinct functions in stabilization and motility of ependymal cilia. *J. Cell Biol.* 202:441–451. http://dx.doi.org/10.1083/jcb.201305041

Bosch Grau, M., C. Masson, S. Gadadhar, C. Rocha, O. Tort, P. Marques Sousa, S. Vacher, I. Bieche, and C. Janke. 2017. Alterations in the balance of tubulin glycylation and glutamylation in photoreceptors leads to retinal degeneration. *J. Cell Sci.* 130:938–949. http://dx.doi.org/10.1242/jcs.199091

Bré, M.H., V. Redeker, M. Quibell, J. Darmanaden-Delorme, C. Bressac, J. Cosson, P. Huitorel, J.M. Schmitter, J. Rossler, T. Johnson, et al. 1996. Axonemal tubulin polyglycylation probed with two monoclonal antibodies: widespread evolutionary distribution, appearance during spermatozoan maturation and possible function in motility. *J. Cell Sci.* 109:727–738.

Bré, M.H., V. Redeker, J. Vinh, J. Rossier, and N. Levilliers. 1998. Tubulin polyglycylation: differential posttranslational modification of dynamic cytoplasmic and stable axonemal microtubules in paramecium. *Mol. Biol. Cell.* 9:2655–2665. http://dx.doi.org/10.1091/mbc.9.9.2655

Callen, A.M., A. Adoutte, J.M. Andrew, A. Baroin-Tourancheau, M.H. Bré, P.C. Ruiz, J.C. Clérot, P. Delgado, A. Fleury, R. Jeanmaire-Wolf, et al. 1994. Isolation and characterization of libraries of monoclonal antibodies directed against various forms of tubulin in *Paramecium*. *Biol. Cell.* 81:95–119. http://dx.doi.org/10.1016/S0248-4900(94)80002-2

Czarnecki, P.G., and J.V. Shah. 2012. The ciliary transition zone: from morphology and molecules to medicine. *Trends Cell Biol.* 22:201–210. http://dx.doi.org/10.1016/j.tcb.2012.02.001

Czarnecki, P.G., G.C. Gabriel, D.K. Manning, M. Sergeev, K. Lemke, N.T. Klena, X. Liu, Y. Chen, Y. Li, J.T. San Agustin, et al. 2015. ANKS6 is the critical activator of NEK8 kinase in embryonic situs determination and organ patterning. *Nat. Commun.* 6. http://dx.doi.org/10.1038/ncomms7023

Davenport, J.R., A.J. Watts, V.C. Roper, M.J. Croyle, T. van Groen, J.M. Wyss, T.R. Nagy, R.A. Kesterson, and B.K. Yoder. 2007. Disruption of intraflagellar transport in adult mice leads to obesity and slow-onset cystic kidney disease. *Curr. Biol.* 17:1586–1594. http://dx.doi.org/10.1016/j.cub.2007.08.034

Delgehyr, N., A. Meunier, M. Faucourt, M. Bosch Grau, L. Strehl, C. Janke, and N. Spassky. 2015. Ependymal cell differentiation, from monociliated to multiciliated cells. *Methods Cell Biol.* 127:19–35. http://dx.doi.org/10.1016/bs.mcb.2015.01.004

Delling, M., P.G. DeCaen, J.F. Doerner, S. Febvay, and D.E. Clapham. 2013. Primary cilia are specialized calcium signalling organelles. *Nature.* 504:311–314. http://dx.doi.org/10.1038/nature12833

Eddé, B., J. Rossier, J.P. Le Caer, E. Desbruyères, F. Gros, and P. Denoulet. 1990. Posttranslational glutamylation of alpha-tubulin. *Science.* 247:83–85. http://dx.doi.org/10.1126/science.1967194

Fry, A.M., M.J. Leaper, and R. Bayliss. 2014. The primary cilium: guardian of organ development and homeostasis. *Organogenesis.* 10:62–68. http://dx.doi.org/10.4161/org.28910

Han, Y.-G., and A. Alvarez-Buylla. 2010. Role of primary cilia in brain development and cancer. *Curr. Opin. Neurobiol.* 20:58–67. http://dx.doi.org/10.1016/j.conb.2009.12.002

Hildebrandt, F., T. Benzing, and N. Katsanis. 2011. Ciliopathies. *N. Engl. J. Med.* 364:1533–1543. http://dx.doi.org/10.1056/NEJMra1010172

Huber, C., and V. Cormier-Daire. 2012. Ciliary disorder of the skeleton. *Am. J. Med. Genet. C. Semin. Med. Genet.* 160C:165–174. http://dx.doi.org/10.1002/ajmg.c.31336

Ikegami, K., D. Horigome, M. Mukai, I. Livnat, G.R. MacGregor, and M. Setou. 2008. TTLL10 is a protein polyglycylase that can modify nucleosome assembly protein 1. *FEBS Lett.* 582:1129–1134. http://dx.doi.org/10.1016/j.febslet.2008.02.079

Janke, C. 2014. The tubulin code: molecular components, readout mechanisms, and functions. *J. Cell Biol.* 206:461–472. http://dx.doi.org/10.1083/jcb.201406055

Konno, A., M. Setou, and K. Ikegami. 2012. Ciliary and flagellar structure and function—their regulations by posttranslational modifications of axonemal tubulin. *Int. Rev. Cell Mol. Biol.* 294:133–170. http://dx.doi.org/10.1016/B978-0-12-394305-7.00003-3

Lahaye, X., T. Satoh, M. Gentili, S. Cerboni, C. Conrad, I. Hurbain, A. El Marjou, C. Lacabaratz, J.-D. Lelièvre, and N. Manel. 2013. The capsids of HIV-1 and HIV-2 determine immune detection of the viral cDNA by the innate sensor cGAS in dendritic cells. *Immunity.* 39:1132–1142. http://dx.doi.org/10.1016/j.immuni.2013.11.002

Lalle, M., A.M. Salzano, M. Crescenzi, and E. Pozio. 2006. The Giardia duodenalis 14-3-3 protein is post-translationally modified by phosphorylation and polyglycylation of the C-terminal tail. *J. Biol. Chem.* 281:5137–5148. http://dx.doi.org/10.1074/jbc.M509673200

Lancaster, M.A., J. Schroth, and J.G. Gleeson. 2011. Subcellular spatial regulation of canonical Wnt signalling at the primary cilium. *Nat. Cell Biol.* 13:700–707. http://dx.doi.org/10.1038/ncb2259

Levilliers, N., A. Fleury, and A.M. Hill. 1995. Monoclonal and polyclonal antibodies detect a new type of post-translational modification of axonemal tubulin. *J. Cell Sci.* 108:3013–3028.

Magiera, M.M., and C. Janke. 2013. Investigating tubulin posttranslational modifications with specific antibodies. *In* Methods in Cell Biology. Vol. 115. J.J. Correia and L. Wilson, editors. Academic Press, Burlington, MA. 247–267. http://dx.doi.org/10.1016/B978-0-12-407757-7.00016-5

Malicki, J.J., and C.A. Johnson. 2017. The cilium: cellular antenna and central processing unit. *Trends Cell Biol.* 27:126–140.

Mary, J., V. Redeker, J.P. Le Caer, J. Rossier, and J.M. Schmitter. 1996. Posttranslational modifications in the C-terminal tail of axonemal tubulin from sea urchin sperm. *J. Biol. Chem.* 271:9928–9933. http://dx.doi.org/10.1074/jbc.271.17.9928

Michaud, E.J., and B.K. Yoder. 2006. The primary cilium in cell signaling and cancer. *Cancer Res.* 66:6463–6467. http://dx.doi.org/10.1158/0008-5472.CAN-06-0462

Mick, D.U., R.B. Rodrigues, R.D. Leib, C.M. Adams, A.S. Chien, S.P. Gygi, and M.V. Nachury. 2015. Proteomics of primary cilia by proximity labeling. *Dev. Cell.* 35:497–512. http://dx.doi.org/10.1016/j.devcel.2015.10.015

Miyoshi, K., K. Kasahara, I. Miyazaki, and M. Asanuma. 2009. Lithium treatment elongates primary cilia in the mouse brain and in cultured cells. *Biochem. Biophys. Res. Commun.* 388:757–762. http://dx.doi.org/10.1016/j.bbrc.2009.08.099

Miyoshi, K., K. Kasahara, I. Miyazaki, and M. Asanuma. 2011. Factors that influence primary cilium length. *Acta Med. Okayama.* 65:279–285.

Multigner, L., I. Pignot-Paintrand, Y. Saoudi, D. Job, U. Plessmann, M. Rüdiger, and K. Weber. 1996. The A and B tubules of the outer doublets of sea urchin sperm axonemes are composed of different tubulin variants. *Biochemistry.* 35:10862–10871. http://dx.doi.org/10.1021/bi961057u

Nager, A.R., J.S. Goldstein, V. Herranz-Pérez, D. Portran, F. Ye, J.M. Garcia-Verdugo, and M.V. Nachury. 2017. An actin network dispatches ciliary GPCRs into extracellular vesicles to modulate signaling. *Cell.* 168:252–263.e14. http://dx.doi.org/10.1016/j.cell.2016.11.036

Overgaard, C.E., K.M. Sanzone, K.S. Spiczka, D.R. Sheff, A. Sandra, and C. Yeaman. 2009. Deciliation is associated with dramatic remodeling of epithelial cell junctions and surface domains. *Mol. Biol. Cell.* 20:102–113. http://dx.doi.org/10.1091/mbc.E08-07-0741

Pathak, N., C.A. Austin, and I.A. Drummond. 2011. Tubulin tyrosine ligase-like genes *ttll3* and *ttll6* maintain zebrafish cilia structure and motility. *J. Biol. Chem.* 286:11685–11695. http://dx.doi.org/10.1074/jbc.M110.209817

Plessmann, U., and K. Weber. 1997. Mammalian sperm tubulin: an exceptionally large number of variants based on several posttranslational modifications. *J. Protein Chem.* 16:385–390. http://dx.doi.org/10.1023/A:1026332621215

Plotnikova, O.V., E.N. Pugacheva, and E.A. Golemis. 2009. Primary cilia and the cell cycle. *Methods Cell Biol.* 94:137–160. http://dx.doi.org/10.1016/S0091-679X(08)94007-3

Redeker, V., N. Levilliers, J.M. Schmitter, J.P. Le Caer, J. Rossier, A. Adoutte, and M.H. Bré. 1994. Polyglycylation of tubulin: a posttranslational modification in axonemal microtubules. *Science.* 266:1688–1691. http://dx.doi.org/10.1126/science.7992051

Redeker, V., N. Levilliers, E. Vinolo, J. Rossier, D. Jaillard, D. Burnette, J. Gaertig, and M.H. Bré. 2005. Mutations of tubulin glycylation sites reveal cross-talk between the C termini of α- and β-tubulin and affect the ciliary matrix in *Tetrahymena*. *J. Biol. Chem.* 280:596–606. http://dx.doi.org/10.1074/jbc.M408324200

Rocha, C., L. Papon, W. Cacheux, P. Marques Sousa, V. Lascano, O. Tort, T. Giordano, S. Vacher, B. Lemmers, P. Mariani, et al. 2014. Tubulin glycylases are required for primary cilia, control of cell proliferation and tumor development in colon. *EMBO J.* 33:2247–2260. http://dx.doi.org/10.15252/embj.201488466

Rogowski, K., F. Juge, J. van Dijk, D. Wloga, J.-M. Strub, N. Levilliers, D. Thomas, M.H. Bré, A. Van Dorsselaer, J. Gaertig, and C. Janke. 2009. Evolutionary divergence of enzymatic mechanisms for posttranslational

polyglycylation. *Cell.* 137:1076–1087. http://dx.doi.org/10.1016/j.cell.2009.05.020

Rüdiger, M., U. Plessman, K.D. Klöppel, J. Wehland, and K. Weber. 1992. Class II tubulin, the major brain beta tubulin isotype is polyglutamylated on glutamic acid residue 435. *FEBS Lett.* 308:101–105. http://dx.doi.org/10.1016/0014-5793(92)81061-P

Rüdiger, M., U. Plessmann, A.H. Rüdiger, and K. Weber. 1995. Beta tubulin of bull sperm is polyglycylated. *FEBS Lett.* 364:147–151. http://dx.doi.org/10.1016/0014-5793(95)00373-H

Schneider, A., U. Plessmann, and K. Weber. 1997. Subpellicular and flagellar microtubules of Trypanosoma brucei are extensively glutamylated. *J. Cell Sci.* 110:431–437.

Spassky, N., F.T. Merkle, N. Flames, A.D. Tramontin, J.M. García-Verdugo, and A. Alvarez-Buylla. 2005. Adult ependymal cells are postmitotic and are derived from radial glial cells during embryogenesis. *J. Neurosci.* 25:10–18. http://dx.doi.org/10.1523/JNEUROSCI.1108-04.2005

Thompson, C.L., A. Wiles, C.A. Poole, and M.M. Knight. 2016. Lithium chloride modulates chondrocyte primary cilia and inhibits Hedgehog signaling. *FASEB J.* 30:716–726. http://dx.doi.org/10.1096/fj.15-274944

Tobin, J.L., and P.L. Beales. 2009. The nonmotile ciliopathies. *Genet. Med.* 11:386–402. http://dx.doi.org/10.1097/GIM.0b013e3181a02882

Tort, O., S. Tanco, C. Rocha, I. Bièche, C. Seixas, C. Bosc, A. Andrieux, M.-J. Moutin, F.X. Avilés, J. Lorenzo, and C. Janke. 2014. The cytosolic carboxypeptidases CCP2 and CCP3 catalyze posttranslational removal of acidic amino acids. *Mol. Biol. Cell.* 25:3017–3027. http://dx.doi.org/10.1091/mbc.E14-06-1072

van Dijk, J., K. Rogowski, J. Miro, B. Lacroix, B. Eddé, and C. Janke. 2007. A targeted multienzyme mechanism for selective microtubule polyglutamylation. *Mol. Cell.* 26:437–448. http://dx.doi.org/10.1016/j.molcel.2007.04.012

Vinh, J., D. Loyaux, V. Redeker, and J. Rossier. 1997. Sequencing branched peptides with CID/PSD MALDI-TOF in the low-picomole range: application to the structural study of the posttranslational polyglycylation of tubulin. *Anal. Chem.* 69:3979–3985. http://dx.doi.org/10.1021/ac970449j

Waters, A.M., and P.L. Beales. 2011. Ciliopathies: an expanding disease spectrum. *Pediatr. Nephrol.* 26:1039–1056. http://dx.doi.org/10.1007/s00467-010-1731-7

Weber, K., A. Schneider, N. Müller, and U. Plessmann. 1996. Polyglycylation of tubulin in the diplomonad *Giardia lamblia*, one of the oldest eukaryotes. *FEBS Lett.* 393:27–30. http://dx.doi.org/10.1016/0014-5793(96)00848-4

Wloga, D., D.M. Webster, K. Rogowski, M.H. Bré, N. Levilliers, M. Jerka-Dziadosz, C. Janke, S.T. Dougan, and J. Gaertig. 2009. TTLL3 Is a tubulin glycine ligase that regulates the assembly of cilia. *Dev. Cell.* 16:867–876. http://dx.doi.org/10.1016/j.devcel.2009.04.008

Wong, S.Y., A.D. Seol, P.-L. So, A.N. Ermilov, C.K. Bichakjian, E.H. Epstein Jr., A.A. Dlugosz, and J.F. Reiter. 2009. Primary cilia can both mediate and suppress Hedgehog pathway-dependent tumorigenesis. *Nat. Med.* 15:1055–1061. http://dx.doi.org/10.1038/nm.2011

Xia, L., B. Hai, Y. Gao, D. Burnette, R. Thazhath, J. Duan, M.H. Bré, N. Levilliers, M.A. Gorovsky, and J. Gaertig. 2000. Polyglycylation of tubulin is essential and affects cell motility and division in *Tetrahymena thermophila*. *J. Cell Biol.* 149:1097–1106. http://dx.doi.org/10.1083/jcb.149.5.1097

Xie, R., K.M. Clark, and M.A. Gorovsky. 2007. Endoplasmic reticulum retention signal-dependent glycylation of the Hsp70/Grp170-related Pgp1p in *Tetrahymena*. *Eukaryot. Cell.* 6:388–397. http://dx.doi.org/10.1128/EC.00366-06

Supplemental material JCB

Gadadhar et al., https://doi.org/10.1083/jcb.201612050

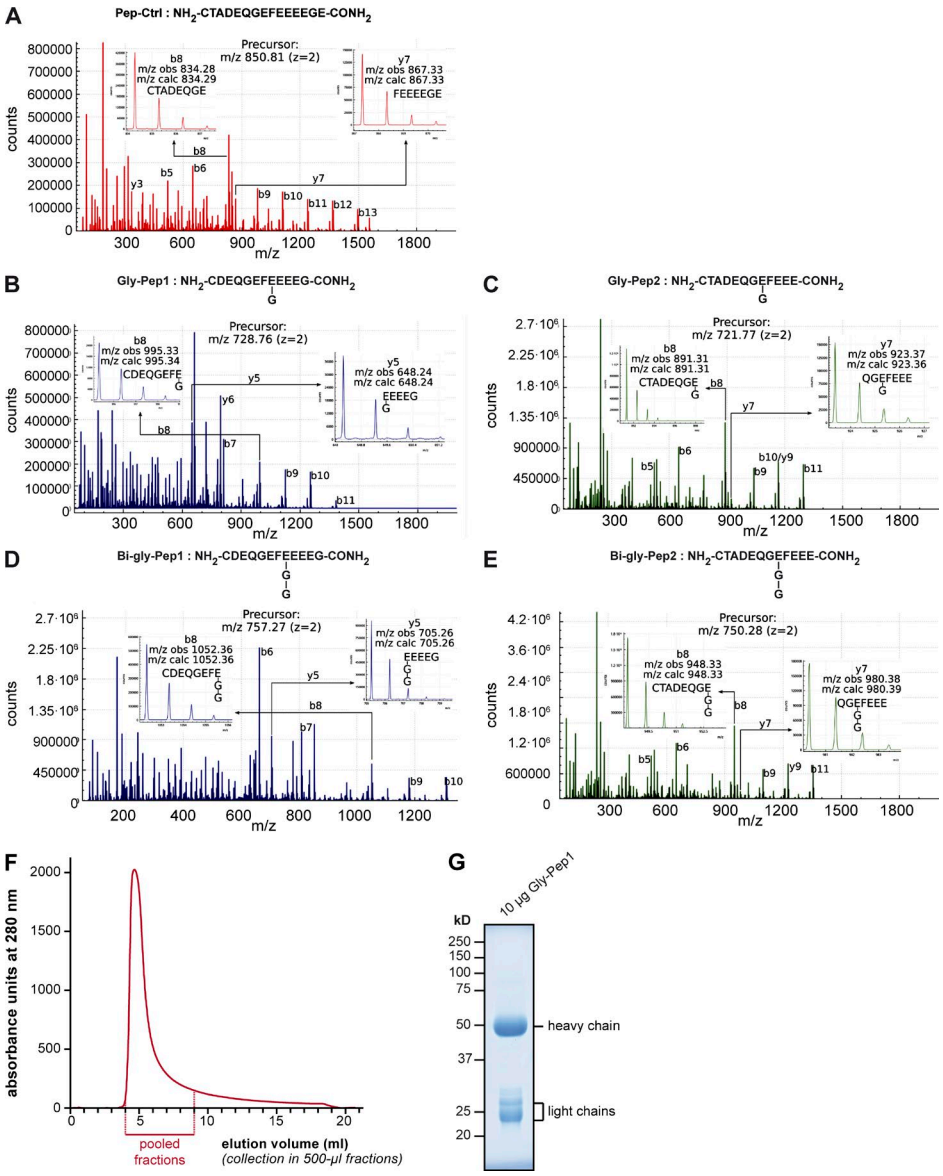

Figure S1. **Validation of the newly synthesized glycylated peptides and the purified gly-pep1 antibody.** (A–E) Synthetic β2-tubulin C-terminal–tail peptides were analyzed by tandem mass spectrometric analysis to verify their sequence and glycylation status. A 0.1 mM stock solution of each of the synthetic peptides (A, control-pep; B, gly-pep1; C, gly-pep2; D, bi–gly-pep1; and E, bi–gly-pep2) was prepared from lyophilized powder by dissolving in a 50:50 (vol/vol) solution of acetonitrile/water. For mass spectrometric analysis, the stock solution was further diluted to 1 µM with the same solvent supplemented with 1% formic acid. The peptide solutions were then introduced into a mass spectrometer (Synapt HDMS G2-Si; Waters) by direct infusion at a flow rate of 7 µl/min. Peptide ions were generated by electrospray (microspray) in standard ion source conditions for peptidic analytes. The double-charged ions were quadrupole selected as precursor ions, and the collision energy was increased to 20–25 V. Collision-induced dissociation tandem mass spectra were recorded. After in silico fragmentation of each peptide with massXpert (Rusconi, 2009), the theoretical data were matched with the observed mass extracted from the mass spectra using the mMass tool (Strohalm et al., 2010). All the peaks that defined the peptide sequence were labeled, and the peaks that unambiguously defined the glycylation modification are detailed in insets, indicating that all the peptides had the modification at the expected sites. From the mass spectrometry analysis, we found that the theoretical mass/charge (m/z) values matched the observed m/z values for each of the modified peptides (as seen in the insets of each mass spectrogram), confirming the sequence and site of modification for each of the peptides. (F and G) The rabbit polyclonal antibody gly-pep1 was purified on an affinity column, which was generated by coupling the antigenic peptide (gly-pep1) to a HiTrap N-hydroxysuccinimide–activated HP affinity matrix (17-0716-01; GE Healthcare). 2.5 mg of the peptide was resuspended in 1 ml of coupling buffer (200 mM sodium bicarbonate buffer, pH 8.3, and 500 mM NaCl) and incubated at room temperature for 5 min. Meanwhile, the column was washed with 6 ml of ice-cold 1 mM HCl. The peptide was then quickly loaded onto the column, sealed, and incubated for 30 min at room temperature. After the coupling, the column was connected to the AKTA purifier 10 (GE Healthcare) and washed with 30 ml PBS. The free N-hydroxysuccinimide–reactive groups of the resin were then deactivated using a series of washing steps as per the manufacturer's protocol. 20 ml gly-pep1 serum was centrifuged at 66,000 *g* for 30 min at 4°C to remove any cellular debris. The supernatant was filtered through a 0.22-µm filter and then loaded onto the preequilibrated (with PBS) affinity column at a flow rate of 0.2 ml/min overnight at 4°C. The flow-through was collected, and the column was washed with 40 ml PBS at a flow rate of 1 ml/min, followed by 20 ml PBS with 1 M NaCl, and again with 20 ml PBS. The specifically bound antibodies were eluted with elution buffer (100 mM glycine/HCl, pH 2.3) in 500-µl fractions. (F) Elution profile of the antibody (absorbance at 280 nm). The pH was immediately adjusted to pH 8.0 by adding 50 µl of 1 M glycine, pH 9.0, to each fraction. The peak fractions were pooled and dialyzed three times against 1 liter of PBS at 4°C for 6 h. (G) 10 µg of the purified antibody was visualized by SDS-PAGE and Coomassie brilliant blue staining. Note a single band for the antibody heavy chain at ∼50 kD and multiple bands for the light chains at ∼25 kD. The purified antibody was adjusted to 1 mg/ml of final concentration and stored at −20°C.

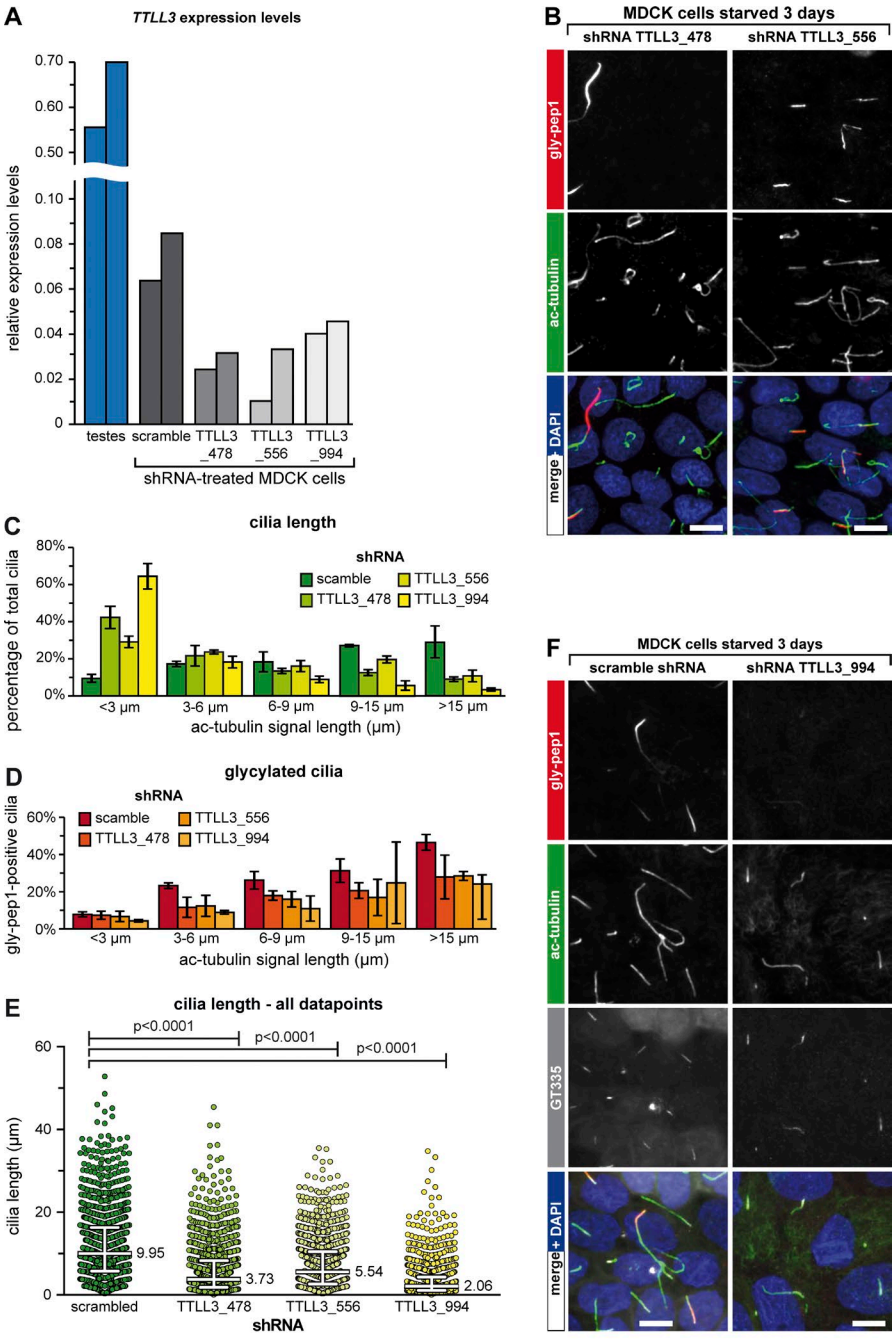

Figure S2. **Extended data for Fig. 5 (A–D): analyses of *TTLL3* knockdown in MDCK cells.** (A) Expression of *TTLL3* was analyzed using quantitative RT-PCR (qRT-PCR). RNA was isolated from MDCK cells 24 h after transduction with lentiviruses coding for shRNAs (scramble, TTLL3_478, TTLL3_556, and TTLL3_994) with TRIzol reagent according to the manufacturer's protocol (Thermo Fisher Scientific). The quality of the RNA was determined by an agarose gel electrophoresis, and RNA was quantified with a spectrophotometer (Nanodrop; Thermo Fisher Scientific). qRT-PCR was performed under standard conditions using the SYBR green master mix kit on the ABI Prism 7900 Sequence Detection System. The relative mRNA expression levels of *TTLL3* were expressed as the N-fold difference in their expression relative to the *TBP* gene. Purified cDNA from dog testes (CliniSciences) was used as a positive control for the qRT-PCR. Data from two independent experiments are shown. Each column represents one individual experiment. Primers used are as follows. For *TTLL3*, we used forward primer 5′-GGTTCGGGGCTCTCTTATTCTCAT-3′ and reverse primer 5′-GCGCACAGAGCTTCATCCACA-3′. For *TBP*, we used forward primer 5′-AAGCTTGACCTAAAGACCATTGCACT-3′ and reverse primer 5′-GGTTCGGGGCTCTCTTATTCTCAT-3′. (B) Immunofluorescence images of 3-d-starved MDCK cells transduced with lentiviruses containing shRNA for *TTLL3* (TTLL3_478 and TTLL3_556). Cilia were stained for glycylation (red) and ac-tubulin (green). The images for scramble and TTLL3_994 shRNA treatment are shown in Fig. 5 A. (C) Extended quantification of the ciliary length distribution as in Fig. 5 B, including data for the TTLL3_478 and TTLL3_556 shRNA treatment. (D) Extended quantification of the percentage of glycylated cilia per length category as in Fig. 5 C, including data for the TTLL3_478 and TTLL3_556 shRNA treatment. (C and D) Each column represents the mean of three independent experiments (±SD). (E) Extended distribution of ciliary lengths and statistics as in Fig. 5 D, including data for TTLL3_478 and TTLL3_556 shRNA treatment. Data are represented as a scatter plot with a line indicating the median (value indicated) and whiskers at interquartile ranges (25th and 75th percentiles). P-values were calculated by one-way ANOVA. Individual experiments are shown in Fig. S3 B. For the number of individual measurements per data point, see Table S1 (n > 1,000). (F) Immunofluorescence images of 3-d-starved MDCK cells transduced with lentiviruses containing scramble and TTLL3_994 shRNA. Cilia were stained for glycylation (red), ac-tubulin (green), and glutamylation (gray). Bars, 10 µm.

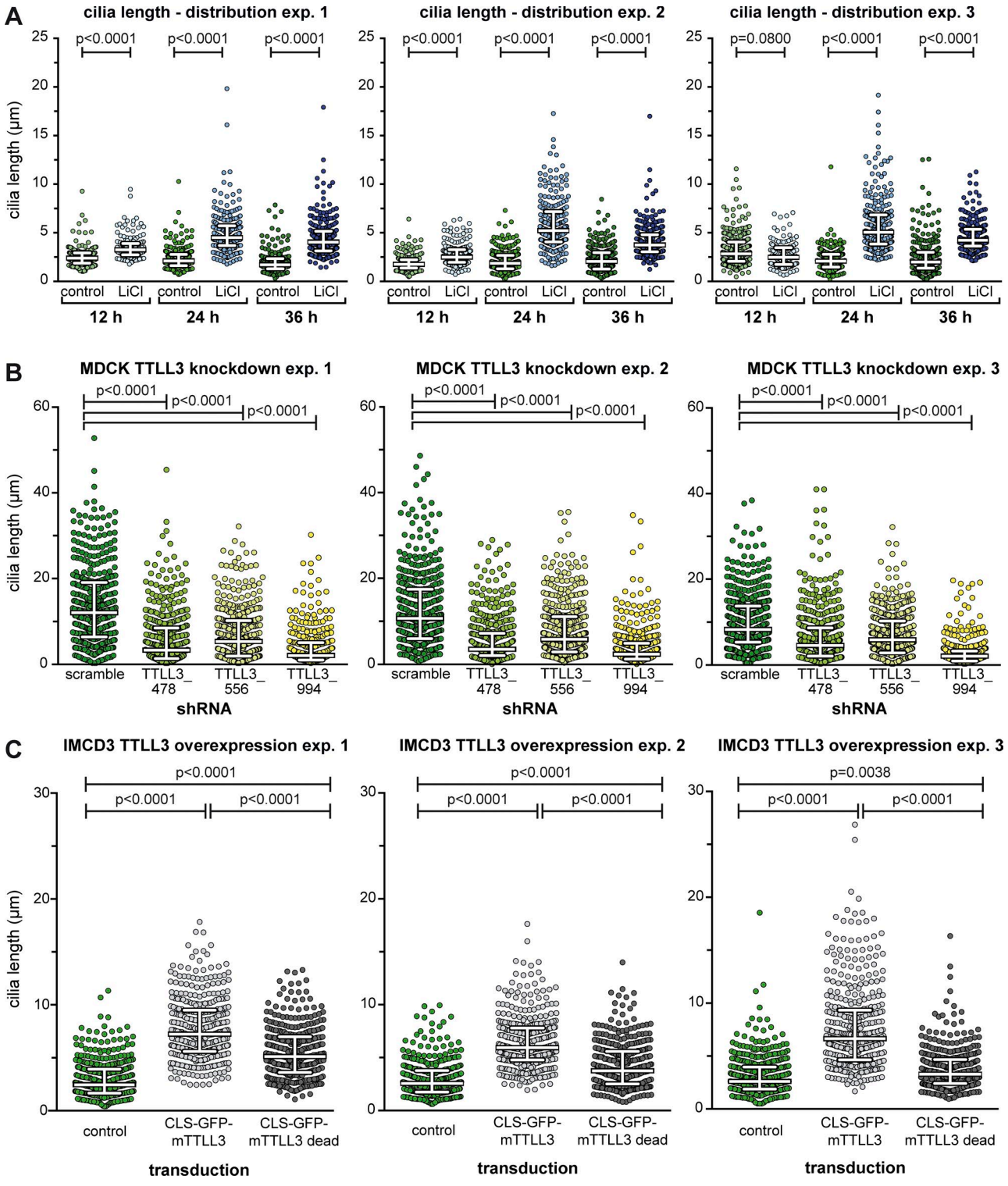

Figure S3. **Extended data for Fig. 4 D, Fig. 5 (D and G), and Fig. S2 E: ciliary length distributions—statistical analyses of individual experiments.** (A) Ciliary length measurements from individual experiments for each experimental condition shown in Fig. 4 A are represented as scatter plots with a line indicating the median (value indicated) and whiskers at interquartile ranges (25th and 75th percentiles). P-values were calculated by one-way ANOVA (combined data: Fig. 4 D). For the number of individual measurements per data point, see Table S1 (n > 100). (B) Ciliary length measurements from individual experiments for each experimental condition shown in Fig. 5 A and Fig. S2 B are represented as scatter plots with a line indicating the median (value indicated) and whiskers at interquartile ranges (25th and 75th percentiles). P-values were calculated by one-way ANOVA (combined data: Fig. S2 E). For the number of individual measurements per data point, see Table S1 (n > 300). (C) Ciliary length measurements from individual experiments for each experimental condition shown in Fig. 5 E are represented as scatter plots with a line indicating the median (value indicated) and whiskers at interquartile ranges (25th and 75th percentiles). P-values were calculated by one-way ANOVA (combined data: Fig. 5 G). For the number of individual measurements per data point, see Table S1 (n > 300).

Table S1 is provided as an Excel file and presents source data for quantification.

References

Rusconi, F. 2009. massXpert 2: a cross-platform software environment for polymer chemistry modelling and simulation/analysis of mass spectrometric data. *Bioinformatics.* 25:2741–2742. http://dx.doi.org/10.1093/bioinformatics/btp504

Strohalm, M., D. Kavan, P. Novák, M. Volný, and V. Havlícek. 2010. mMass 3: a cross-platform software environment for precise analysis of mass spectrometric data. *Anal. Chem.* 82:4648–4651. http://dx.doi.org/10.1021/ac100818g